System Matrix Modeling of Externally Tracked Motion

A. Rahmim, J. C. Cheng, K. Dinelle, M. Shilov, W. P. Segars, O. G. Rousset, B. M. W. Tsui, D. F. Wong, V. Sossi

***Abstract*— In high resolution emission tomography imaging, even small patient movements can considerably degrade image quality. This work investigates an approach to motion compensated reconstruction of motion-contaminated data, thus applicable to *any* scanner in the field (e.g. without list-mode acquisition capability), assuming externally-tracked motion information; it involves incorporation of the measured motion information into the system matrix of the EM algorithm. Furthermore, it is shown that the effect of motion-contamination of the attenuation factors should also be modeled and taken into account in the reconstruction task.**

I. Introduction and Motivation

With continuous improvements in spatial resolution of emission tomography scanners, small patient movements become a significant source of resolution degradation. There has been an increased tendency *not* to exclusively rely on the emission data itself for the estimation of patient movements. More successful approaches instead make use of information provided by an external motion-tracking device. These include:

(1) Use of multiple acquisition frames (MAFs) [1] which are individually reconstructed, motion-compensated and summed: the major limitation of the MAF approach is that lowering the motion threshold can result in the acquisition of an increasing number of *low-statistic* frames to be reconstructed.

(2) Post-processing of the motion-blurred reconstructed images using de-convolution operators (whose shape is determined by the measured motion) [2]. This method, however, has not attracted much attention primarily because the de-convolution process amplifies the noise in the PET data.

(3) Correcting individual lines-of-response (LORs) for motion [3]. It has been argued (e.g. see [4]) that this approach (in its purely event-driven form) may result in reconstructed image artifacts. This is because an LOR that is normally in the field-of-view (FoV) can fall outside the FoV due to motion, and therefore the reconstruction algorithm should be modified in order to yield accurately reconstructed images. However, this approach requires either (i) specialized hardware to achieve accurate on-the-fly motion correction or (ii) list-mode acquisition capability. In this work, our primary interest has been on the investigation of an approach to the reconstruction of motion-compensated data, thus applicable to *any* scanner in the field (e.g. without the list-mode acquisition capability).

(4) As a solution to the above interest, a method [5] models motion blurring in the forward-projection step of the EM algorithm, such that better matching of the estimated image and the motion-contaminated data are obtained. This method, however, does not represent accurate modeling of the motion process, as shown in this work, can result in artifacts and is not necessarily convergent. A more comprehensive approach avoiding the aforementioned difficulties is proposed and investigated.

A. Rahmim, O. G. Rousset and D. F. Wong are with the Division of Nuclear Medicine, Department of Radiology, Johns Hopkins University, Baltimore MD 21205 (e-mail arahmim1@jhmi.edu, pvcorrection@yahoo.com, dfwong@jhmi.edu).

J. C. Cheng, K. Dinelle and V. Sossi are with the Department of Physics and Astronomy, University of British Columbia, Vancouver BC V6T 1Z1 (e-mail kdinelle@phas.ubc.ca, jcheng@phas.ubc.ca, vesna@phas.ubc.ca).

M. Shilov, W. P. Segars and B. M. W. Tsui are with Division of Med. Imaging Physics, Depart.of Radiology, Johns Hopkins University, Baltimore MD 21205 (e-mail mshilov1@jhmi.edu, wsegars1@jhmi.edu, btsui1@jhmi.edu).

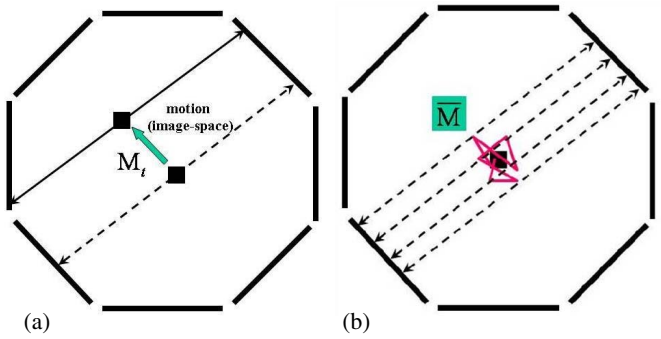

Fig. 1. (a) The operator $\mathbf{M}_t$ tracks movements of the image elements at each time/motion-frame t. (b) The overall weighted motion matrix $\bar{\mathbf{M}}$ models the overall motion-induced blurring (in image-space), thus accurately modeling how motion affects the acquired data.

II. Modeling of Motion into the System Matrix

We first divide a given scan (of duration T) into Q motion-related time intervals (t=1...Q) each with a duration ΔT_t within which motion is limited below a small, negligible threshold. We then define an overall motion matrix $\bar{\mathbf{M}}$ to model motion of the object in the image-space, thus relating a voxel j to other positions j' to which it may contribute due to motion. The overall motion matrix $\bar{\mathbf{M}}$ is thus:

$$\bar{\mathbf{M}} = \sum_{t=1}^{Q} \mathbf{M}_t \frac{\Delta T_t}{T} \qquad (1)$$

where $\mathbf{M}_t$ represent the motion matrix for a particular motion interval t, mapping each voxel j to its new position as measured

using external tracking (see Fig. 1).

Next, we decompose the system matrix $\mathbf{P}=(p_{ij})_{I\times J}$ into four components:

$$\mathbf{P} = \mathbf{W}\mathbf{G}\mathbf{B}\bar{\mathbf{M}} \tag{2}$$

Here, the matrix $\mathbf{B}=(b_{ij})_{J\times J}$ accounts for the image-based blurring effects (other than motion); e.g. positron range in PET. The matrix $\mathbf{G}=(g_{ij})_{I\times J}$ contains the geometric probability terms relating each voxel j to an LOR i. Sensitivity variations due to attenuation and normalization can be taken into account using the diagonal elements w_{ii} of the $\mathbf{W}$ operator. For compact representation [6], we use $\vec{s}=[s_1...s_J]^{tr}$, $\vec{n}=[n_1...n_J]^{tr}$, $\vec{\lambda}^m=[\lambda_1^m...\lambda_J^m]^{tr}$ to denote $1D$ vectors of image sensitivity, projection data and image intensity (estimated at iteration m), respectively (tr denotes the transpose). Upon substitution of Eq. (2) into the EM algorithm, one arrives at:

$$\vec{\lambda}^{m+1} = \frac{\vec{\lambda}^m}{\vec{s}} \times \bar{\mathbf{M}}^{tr}\mathbf{B}^{tr}\left[\sum_{i=1}^{I} BP_i\left\{\frac{\vec{n}}{FP_i(\mathbf{B}\bar{\mathbf{M}}\vec{\lambda}^m)}\right\}\right] \tag{3}$$

where vectorial multiplication and division operations are performed on an element-by-element basis, FP_i and BP_i denote geometric operators which perform forward- and back-projection along LOR i, and the sensitivity vector $\vec{s}$ is given by

$$\vec{s} = \bar{\mathbf{M}}^{tr}\mathbf{B}^{tr}\sum_{i=1}^{I} BP_i\{\vec{w}\} \tag{4}$$

where $\vec{w}$ denotes a list of diagonal elements of $\mathbf{W}$.

Here, we note that one needs to apply $\mathbf{B}\bar{\mathbf{M}}$ and $\bar{\mathbf{M}}^{tr}\mathbf{B}^{tr}$ only once in each (subset of) iteration, and *not* for each and every LOR. Additionally, unlike the 'motion deconvolution' technique in [2], this method does not amplify noise since it makes uses of $\bar{\mathbf{M}}$ and $\bar{\mathbf{M}}^{tr}$ (and *not* $\bar{\mathbf{M}}^{-1}$).

It must be noted that modeling the motion information into the system matrix of the EM algorithm, in the context of non-rigid motion, has been previously proposed for the reconstruction of respiratory non-gated data [7] as well as respiratory/cardiac gated data [8], [9], though the latter does not involve motion-contaminated data (as the data are gated, thus different motion modeling is used for each gate). One must also note that estimation of respiratory/cardiac movements requires alternative approaches, including the possibility of extracting the motion information (i) from separately reconstructed PET gated data, or (ii) from gated CT images in PET/CT applications.

The aforementioned modeling of motion into the system matrix of the EM algorithm, investigated in this work, is expected to improve the reconstructed image qualities. In fact, we have argued in [10] that such modeling of image blurring effects not only improves image resolution, but can also improve noise propagation properties in the reconstruction process. This idea is somewhat paralleled in collimator-detector response (CDR) modeling in SPECT, wherein a similar incorporation in the reconstruction process has been shown to result in improvements in resolution [11], in task-based measures of image-quality (see [12] for a review), as well as improvements in noise properties [13].

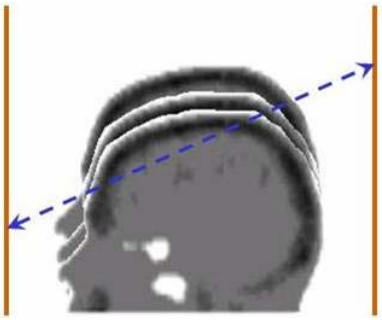

Fig. 2. Attenuation factors along a particular LOR can be modified due to motion.

III. Modeling of Motion for Attenuation Correction

At this stage, one must note the following: in addition to the data, the attenuation coefficients for the LORs are also contaminated by motion. In other words, the probability of attenuation along an LOR is modified due to motion, as shown in Fig. 2. We thus introduce an operator $\mathcal{L}_t()$ which models the effect of motion in the LOR-space by transforming the LOR i along which an event *would* have been detected to the LOR i' along which the event *is* detected during interval t. Next, defining $\mathbf{N}$ and $\mathbf{A}_t$ as diagonal matrices incorporating the normalization and (time-dependent) attenuation factors, the latter's diagonal elements $a_{ii}^{(t)}$ are given by

$$a_{ii}^{(t)} = a_{ll}^{(0)} \quad \text{with} \quad l = \mathcal{L}_t^{-1}(i) \tag{5}$$

where $a_{ll}^{(0)}$ represents the attenuation factors for the object scanned at initial position. The overall system matrix is then accurately given by

$$\mathbf{P} = \sum_{t=1}^{Q} \mathbf{A}_t\mathbf{N}\mathbf{G}\mathbf{B}\mathbf{M}_t \times \frac{\Delta T_t}{T} \tag{6}$$

For high-resolution scanners, the above summation over all the motion frames will be computationally intense: this is because while $\mathbf{M}_t$ and $\mathbf{A}_t$ are individually sparse, the above collective term is very non-sparse. We therefore introduce the following simplification: due to the relatively broad distribution of attenuation factors, we assume that the term $\mathbf{A}_t$ in (6) can be replaced by a motion averaged term $\bar{\mathbf{A}}$ resulting in:

$$\mathbf{P} = \sum_{t=1}^{Q} \bar{\mathbf{A}}\mathbf{N}\mathbf{G}\mathbf{B}\mathbf{M}_t \times \frac{\Delta T_t}{T} = \bar{\mathbf{A}}\mathbf{N}\mathbf{G}\mathbf{B}\bar{\mathbf{M}} \tag{7}$$

In order to calculate $\bar{\mathbf{A}}$, we then note that the measured mu-map $\vec{\mu}(0)$ undergoes motion in the course of the scan as given by:

$$\vec{\mu}(t) = \mathbf{M}_t\vec{\mu}(0) \tag{8}$$

Thus, the effective, overall mu-map $\overline{\vec{\mu}}$ is given by:

$$\overline{\vec{\mu}} = \sum_{t=1}^{Q} \vec{\mu}(t) \times \frac{\Delta T_t}{T} = \sum_{t=1}^{Q} \mathbf{M}_t\vec{\mu}^{(0)} \times \frac{\Delta T_t}{T} \tag{9}$$

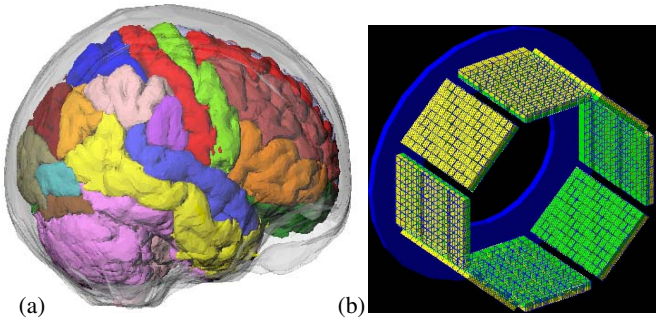

(a) (b)

Fig. 3. (a) New Mathematical Brain Phantom. (b) HRRT scanner geometry used in the combined SimSET/GATE simulation for the HRRT scanner.

This term is easily computed, and can be forwarded projected to yield the motion-weighted attenuation factors (i.e. elements of $\bar{\mathbf{A}}$).

IV. Simulations of a New Mathematical Brain Phantom

Our emphasis in this work has been to compare and validate motion compensation methods under realistic imaging scenarios. The tools developed in this regard have been two-fold:

1) *A New mathematical brain phantom:* Voxelized phantoms are problematic in that they are fixed to a particular spatial resolution, and also result in *interpolation errors* when modeling motion (e.g. the volume of a voxelized object may not be conserved after rotation). Alternatively, a mathematical brain phantom was developed, as depicted in Fig. (3a). The brain phantom was constructed using subdivision surfaces [14]. Surfaces were modeled based on a segmented MRI dataset of a normal subject. One-hundred structures in the brain were identified. A software application was written using the Visualization Toolkit (VTK) [15] to create 3D polygon surfaces, which were then used to generate subdivision surfaces as described by Hoppe et al. [14].

2) *PET Simulations:* A new technique [16] was used involving combination of two powerful and well-validated Monte-Carlo codes, SimSET and GATE. The method takes advantage of the shorter simulation times for photon propagation inside a digital phantom using SimSET as compared to GATE. We used the design parameters and the geometry of the second generation HRRT scanner, as depicted in Fig. (3b). The total simulation times using the new technique are about 12 times faster with nearly similar accuracy.

V. Methods, Results and Discussion

(1) 2D Simulations and Analysis: as a first step, 2D simulations of digitized brain images were considered. The 2D sinograms had 96 projections and 96 bins. Five different positions were simulated, with incremental motions of translating by 1 pixel (width 4.87mm) along both directions and rotating by 1°. The simulated data were reconstructed using the OSEM algorithm (24 subsets). Four motion correction methods were compared: (i) Motion incorporated in the forward projection step only [5]; FPMM (forward-projection motion modeling). (ii) The proposed System Matrix Modeling of Motion with Conventional Attenuation Correction (SMMM-CAC). (iii) System Matrix Modeling of Motion with Proposed Attenuation Correction (SMMM-PAC).

Quantitative Metrics: Ten *contour ROIs* were defined each consisting of voxels of similar (within 2%) activity. The reconstructed image bias was then measured using an ROI-based normalized mean squared error (NMSE) metric given by:

$$\text{NMSE} = \frac{1}{R}\sum_{r=1}^{R}\left(\frac{\bar{\lambda}_r - \mu_r}{\mu_r}\right)^2 \tag{10}$$

where μ_r and $\bar{\lambda}_r$ denote the true and reconstructed activities over each ROI r. Noise was monitored using the normalized standard deviation (NSD) averaged over the various ROIs:

$$\text{NSD} = \frac{1}{R}\sum_{r=1}^{R}\left(\frac{\sqrt{\frac{1}{n-1}\sum_{j\in r}(\lambda_j - \bar{\lambda}^r)^2}}{\bar{\lambda}^r}\right) \tag{11}$$

where λ_j denotes the estimated activity at voxel j (for a particular iteration number).

The resulting noise (NSD) vs. bias (NMSE) plots are depicted in Fig. (4a,b). We have repeatedly observed that the FPMM method does not perform well. Alternatively, the proposed SMMM-CAC/PAC methods perform well, with the latter exhibiting improved NSD vs. NMSE performance. Visually, a similar improved performance may be observed as shown in Fig. (5).

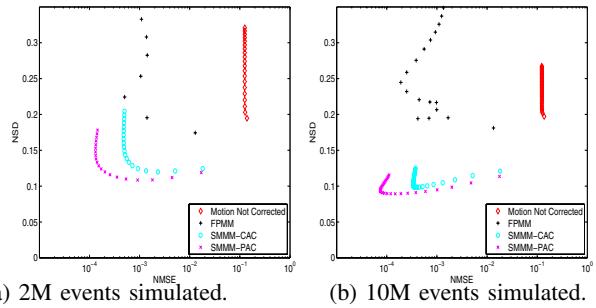

(a) 2M events simulated. (b) 10M events simulated.

Fig. 4. Resulting plots of NSD (noise) vs. NMSE (bias) with different number of iterations.

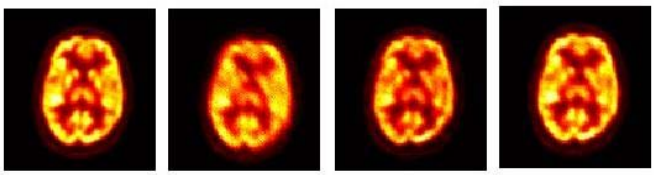

(a) True Image (b) Not corrected (c) SMMM-CAC (d) SMMM-PAC

Fig. 5. Reconstructed images after 10 iterations (24 subsets). Simulation contained 10M events in the sinogram.

(2) 3D Simulations and Analysis: Using the developed tools as discussed in Sec. IV, we performed simulations of our mathematical phantom in the HRRT scanner. A span of 3

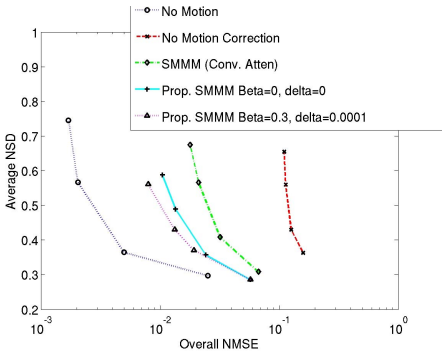

Fig. 6. Resulting plots of NSD (noise) vs. NMSE (bias) for the fully simulated 3D phantom with different number of iterations. Simulation contained 77M events in the sinogram.

and maximum ring difference of 67 were considered. Three different positions were included in the study, with incremental motions each of translating by 7.5mm along both transaxial directions and 10mm along the axial direction. Reconstructions were performed using the OSEM algorithm with 16 subsets. Six different areas in the brain (caudate, putamen, grey, white, cerebellum and brain stem) were quantitatively analyzed, and the NMSE values (for different iterations) were determined as given by Eq. 10, and plotted against the average ROI NSD. The true ROI μ_r values were obtained from the known phantom volumes. The resulting noise vs. bias plots are shown in Fig. (6).

The proposed approach (especially when including modeling of modified attenuation factors due to presence of motion) performs favorably compared to the case with no motion correction. Nevertheless, one observes that, compared to the case with no motion, increasing number of iterations are required to achieve similar bias performance, thus resulting in poorer noise vs. bias. This can be attributed to the fact that in this approach the data is not explicitly corrected for motion, and rather the motion information is incorporated in the reconstruction task of the contaminated data-sets. We have shown a plot when MAP (maximum *a priori*) reconstruction is applied (to suppress noise) somewhat improving the performance, and this is an area that needs to be further investigated and optimized.

Fig. (7) depicts transaxial/coronal/sagittal slices for various reconstructions. Similar conclusions as above can be drawn.

VI. Conclusion

In this work, we have proposed and investigated a motion correction method applicable to *any* scanner in the field (e.g. without the list-mode acquisition capability). It has been demonstrated that in the case of motion-contaminated data, accurate incorporation of tracked motion information into the system matrix of the EM algorithm yields quantitatively and qualitatively improved images. At the same time, we have shown that quantitation is further improved if the effect of motion-contamination on the attenuation factors is further modeled and incorporated in the reconstruction task.

Ongoing work includes using the aforementioned tools to further validate the proposed method in different realistic

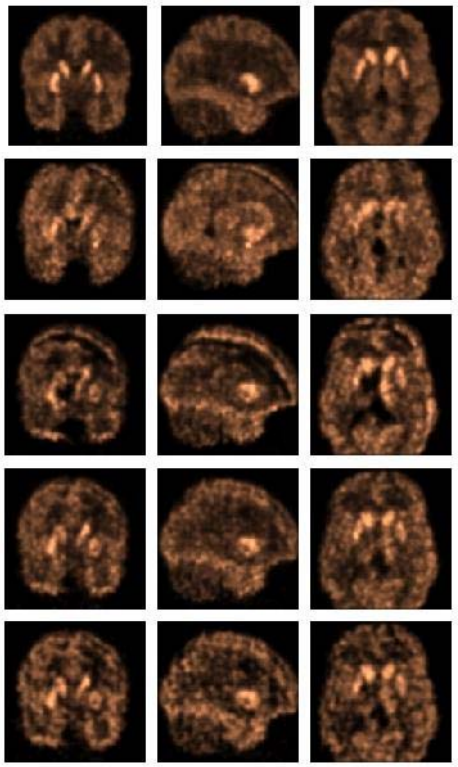

(a) Transaxial (b) Coronal (c) Sagittal

Fig. 7. *Row 1:* No motion. *Row 2:* No motion correction. *Row 3:* SMMM with conventional attenuation correction. *Row 4:* SMMM with the proposed attenuation correction. *Row 5:* Same as above, except with MAP reconstruction.

imaging protocols, with different counting statistics and reconstruction parameters. While in this work, the motion amplitudes have been consistent with realistic measurements, we plan on more closely simulating patient movements, using the recently installed polaris/vicra cameras for our scanners.

Acknowledgments

This work was supported by the National Institute of Health, the TRIUMF Life Science Grant, the Natural Sciences and Engineering Research Council of Canada, and the Michael Smith Foundation for Health Research. The authors wish to especially thank Andrew Crabb, Kelvin Raywood and Ken Buckley for computational and technical support.

References

[1] R. R. Fulton, S. R. Meikle, S. Eberl, J. Pfeiffer, and C. J. Constable, "Correction for head movement in positron emission tomography using an optical motion tracking system", *IEEE Trans. Nucl. Sci.*, vol. 49, pp. 116-123, 2002.

[2] M. Menke, M. S. Atkins, and K. R. Buckley, "Compensation Methods for Head Motion Detected During PET Imaging", *IEEE Trans. Nucl. Sci.*, vol. 43(1), pp. 310-317, 1996.

[3] M. E. Daube-Witherspoon, Y. C. Yan, M. V. Green, R. E. Carson, K. M. Kempner, and P. Herscovitch, "Correction for motion distortion in PET by dynamic monitoring of patient position (Abstract)", *J. Nucl. Med.*, vol. 31, pp. 816, 1990.

[4] A. Rahmim, P. Bloomfield, S. Houle, M. Lenox, C. Michel, K. R. Buckley, T. J. Ruth, and V. Sossi, "Motion compensation in histogram-mode and list-mode EM reconstructions: beyond the event-driven approach", *IEEE Trans. Nucl. Sci.*, vol. 51, pp. pp. 2588-2596 (2004).

[5] R. R. Fulton and S. R. Meikle, "Reconstruction of Projection Data Corrupted by Rigid or Non-Rigid Motion", oral presentation at *IEEE Med. Imag. Conf*, 2005.
[6] A. J. Reader, S. Ally, F. Bakatselos, Roido Manavaki, R. Walledge, A.P.Jeavons, P.J.Julyan, S.Zhao, D. L. Hastings and Jamal Zweit, "One-Pass List-Mode EM Algorithm for High-Resolution 3-D PET Image Reconstruction Into Large Arrays", *IEEE Trans. Nucl. Sci.* vol. 49, pp. 693-699, 2002.
[7] M. Reyes, G. Malandain, P. M. Koulibaly, and J. Darcourt, "Respiratory Motion Correction in Emission Tomography Imaging" *Proceed. 8th Intern. Meeting. Fully 3D Image Recon. Radiol. Nucl. Med.*, pp. 110-113, 2005.
[8] F. Qiao, T. Pan, J. W. Clark, O. R. Mawlawi, "Motion-Incorporated Reconstruction Method for Gated PET Studies", *Phys. Med. Biol.*, pp. 3769-3783, 2006.
[9] T. Li, B. Thorndyke, E. Schreibmann, Y. Yang, and L. Xing, "Model-based image reconstruction for four-dimensional PET" *Med. Phys. Vol.*, vol. 33, pp. 1288-1298, 2006.
[10] Rahmim A, Cheng JC, and V. Sossi, "Improved noise propagation in statistical image reconstruction with resolution modeling", *IEEE Med. Imag. Conf. Records*, 2005.
[11] Kohli V, King MA, Glick SJ et al. Comparison of frequency-distance relationship and Gaussian-diffusion based methods of compensation for distance-dependent spatial resolution in SPECT imaging. Phys. Med. Biol. 1998; 43: 1025-1037.
[12] Frey EC, Tsui BMW. Collimator-Detector Response Compensation in SPECT (chapter 5) In Quantitative Analysis in Nuclear Medicine Imaging. Zaidi H. (Ed.) New York: Springer. 2006.
[13] Tsui BMW, Frey EC, Zhao XD et al. The importance and implementation of accurate three-dimensional compensation methods for quantitative SPECT. Phys. Med. Biol. 1994; 39: 509-530.
[14] H. Hoppe, T. DeRose, T. Duchamp, M. Halstead, H. Jin, J. McDonald, J. Schweitzer, W. Stuetzle, "Piecewise smooth surface reconstruction", Computer Graphics, vol. 28, pp. 295-302, 1994.
[15] The Visualization Toolkit, http://public.kitware.com/VTK
[16] M. A. Shilov, E. C. Frey, W. P. Segars, J. Xu, and B. M. W. Tsui, "Improved Monte-Carlo Simulations for Dynamic PET", society of nuclear medicine publication, 2006.